J Therm Anal Calorim (2017) 127:2093–2099
DOI 10.1007/s10973-016-5724-z

New approach of synthesis of phosphate–sulfates with NZP-type structure

V. I. Pet'kov[1] · A. S. Dmitrienko[1] · M. V. Sukhanov[1] · A. M. Kovalskii[2]

Received: 16 March 2016 / Accepted: 15 July 2016 / Published online: 28 July 2016

Abstract New approach of phosphate–sulfate synthesis, preventing sulfur elimination was proposed. It implies sulfur encasement into intermediate with heightened thermal resistance, thus the synthesis temperature of phosphate–sulfate could be increased, and crystallization can be performed. This method is considered to be capable by example of obtaining of $Pb_{2/3}FeZr(PO_4)_{7/3}(SO_4)_{2/3}$ ceramic. It was synthesized by means of sol–gel method via formation of intermediate $PbSO_4$, which encased sulfur and eventually led to formation of mentioned before phosphate–sulfate. Obtained sample was characterized via X-ray, IR, combined DTA–TG, SEM and microprobe electron analysis. Crystal structure and unit cell parameters were derived from least-squares refinement of powder X-ray diffraction data (NZP-type, sp. gr.$R\bar{3}c$, $a = 8.6339$ Å, $c = 23.2991$ Å, $V = 1504.1$ Å^3). Thermal expansion ($\alpha_a = 0.96{\cdot}10^{-6}$, $\alpha_c = 3.24{\cdot}10^{-6}$, $\alpha_{av} = 1.76{\cdot}10^{-6}$ K^{-1}) of compound also has been studied. There is a wide area of interest, due to development of ceramics with low thermal expansion.

✉ V. I. Pet'kov
petkov@inbox.ru

[1] Lobachevsky State University of Nizhni Novgorod, Gagarin Av. 23, Nizhni Novgorod, Russia 603950

[2] National University of Science and Technology "MISIS", Leninskii Av. 4, Moscow, Russia 119049

Graphical Abstract

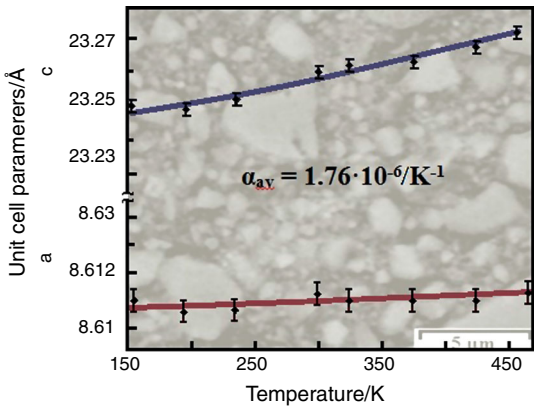

Keywords Phosphate–sulfate · Sol–gel method · Thermal analysis · Characterization · Thermal expansion

Introduction

Materials–structural analogues with the mineral kosnarite, $KZr_2(PO_4)_3$ [1], including large family of NASICON, $Na_{1+x}Zr_2Si_xP_{3-x}O_{12}$ solid ionic conductors [2], and $NaZr_2(PO_4)_3$ (NZP) [3], have attracted researchers attention due to their high ionic conductivity [4], low thermal expansion [5] and high resistance toward damage under natural corrosion conditions [6]. These properties allow them to be used in the fabrication of various products: ceramic electrolytes, thermal shock resistant ceramics, semiconductor substrates, catalyst supports and host matrices for secure toxic/radioactive waste immobilization [3, 7–9]. In accordance with detailed knowledge about compound structure, synthesis of superionic materials NASICON with low temperatures of cation conductivity via iso- and

heterovalent substitutions can be performed [10–12]. The great interest toward NZP compounds can also be explained by expanding prospects of usage these materials as high-tech ceramics with unique ability to hardly expand in the wide range of temperatures [13, 14]. Due to possible cation and anion substitutions the properties could be considerably modified. There are some approaches how thermal expansion value can be reduced [15–18]. It is well-known fact that behavior under thermal exposure of NZP structure depends on the nature, ratio between size and number of cations, occupying varied crystallographic positions, number of vacant positions and symmetry of unit cell. While compound with NZP structural type ($NaZr_2(PO_4)_3$) is under heating, most feeble bonds Na–O extend much more than the strong bonds Zr–O and P–O (Fig. 1). Size of the trigonal antiprism constructed around Na position (M1 position) increases under heating, so it leads to elongation of column, consisted of polyhedral along *c*-axis ($\alpha_c > 0$). That causes angle distortions in polyhedra via rotation of vertex bound ZrO_6-octahedra and PO_4-tetrahedra. Tetrahedral angle O−P−O increases toward *c*, distance between columns of framework structure decreases and structure shrinks along *a*-axis ($\alpha_a < 0$) [19]. In keeping with mentioned before, average magnitude of thermal expansion coefficient is really low.

Thus, one way of reducing thermal expansion is cation substitution in M1 position (small cations are substituted by big ones). In this case, position can be occupied by cations, which radius is in range from 0.95 to 1.67 Å (K^+, Rb^+, Cs^+, Ca^{2+}, Sr^{2+}, Ba^{2+}, Cd^{2+}) [18]. Another way is substitution of anion forming element (phosphorous) with smaller one (sulfur). This is considered that it reduces cell volume and thermal expansion and can be performed by using cheap elements (K, Pb) in M1 position.

It is well-known fact that in contrast to sulfates, temperatures of phosphate synthesis are rather high [20–22]. This is the main cause of synthesis difficulties of mixed phosphate–sulfates. We attempted to synthesize numerous compounds with alkali metals in M1 position, including row $AZrFe(PO_4)_2SO_4$, A–Li, Na, K, Rb, Cs, yet only compound with sodium was obtained with great extent of purity. Isomorphic substitution

$$Zr^{4+} + P^{5+} \rightarrow Fe^{3+} + S^{6+}$$

in the basic $NaZr_2(PO_4)_3$ leads to $NaFeZr(PO_4)_2SO_4$ formation. But the real synthesis is rather complicated due to multiple cycle repetition "grinding–pressing–heating" and partial loss of sulfur above 873 K. There is the main problem of phosphate–sulfate synthesis caused by partial losses of sulfur as SO_3.

We invented new method, which enables us to avoid sulfur loses during the synthesis of phosphate–sulfates. So it implies sulfur encasement into intermediate reagent with heightened decay temperature. In this case, synthesis temperature could be increased; therefore, phosphate–sulfate crystallization can be easily performed. The main goal of this research is to depict application of that method by example of the phosphate–sulfate $Pb_{2/3}FeZr(PO_4)_{7/3}(SO_4)_{2/3}$. It has been opted, due to stoichiometry ratio between lead and SO_4 anion (1:1), providing formation of stable intermediate $PbSO_4$ (thermally resistant up to 1443 K). Thermal expansion of synthesized compound has been studied in the temperature range 153–473 K.

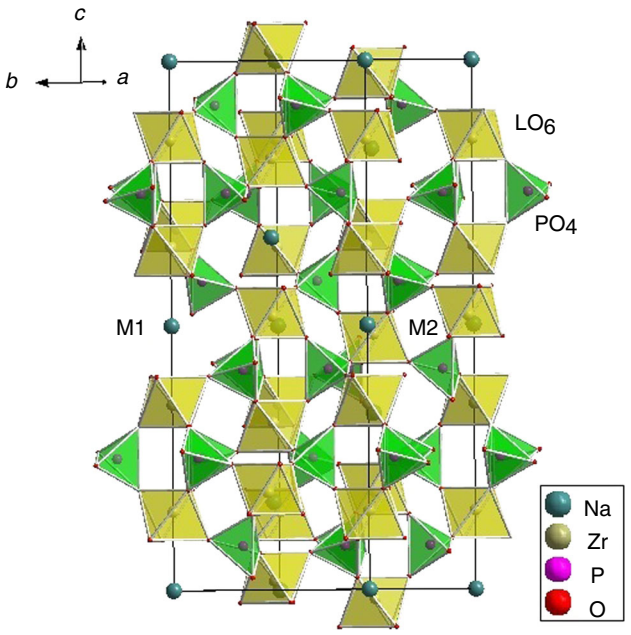

Fig. 1 Crystal structure of NZP ceramics. The framework comprised of L-octahedra and P-tetrahedra. M1, M2—extraframework positions

Experimental

Materials

All chemicals of $Pb(NO_3)_2$, $FeCl_3 \cdot 6H_2O$, $ZrOCl_2 \cdot 8H_2O$, H_3PO_4, H_2SO_4 were provided by "Reachem" and used without further purification. Their purity was not <99.5 %.

Preparation of phosphate–sulfate

$Pb_{2/3}FeZr(PO_4)_{7/3}(SO_4)_{2/3}$ sample was prepared with a sol–gel process. Stoichiometric amounts of 1 M aqueous solutions of lead nitrate(II), iron chloride(III) and zirconium oxychloride were poured together under constant stirring at 293 K; after a while, solutions of sulfuric and orthophosphoric acids were added alternately with stirring. The precursor mixture (gel) was heated at 363 K until full water evaporation. When the dry mixture was obtained, it was subjected to stepwise isothermal heating at 473, 773, 873, 973 and 1023 K for 24 h. Stepwise heating was alternated with grinding in the agate

mortar for 30 min. Obtained phosphate–sulfate was red powder. Then, the powder was pressed into pellet with pressure of 6 MPa, the size of which was 9.6 mm in diameter and 3 mm thickness. Pellet was finally sintered at 1023 K.

Methods

The chemical composition and homogeneity of the sample were checked with X-ray microanalysis on JEOL JSM 7600F field emission (Schottky cathode) scanning electron microscope (SEM). The microscope was equipped with an Oxford Instruments X-Max 80 (Premium) energy-dispersive spectrometer system for X-ray microanalysis, equipped with a semiconductor silicon drift detector. The elemental composition of the sample was determined with an accuracy of 2.0 mol%.

X-ray diffraction patterns were obtained on a Shimadzu XRD-6000 diffractometer (Ni-filtered CuK_α radiation, $\lambda = 1.54178$ Å, angular range $2\theta = 10°$–$110°$). Unit cell parameters were determined after indexing X-ray diffraction patterns. Rietveld method was used for diffraction pattern processing and structure refinement [23, 24]. The peak profiles were approximated by means of modified pseudo-Voight function [25]. The crystal structure was refined by gradually increasing the number of the parameters being refined under continuous graphical modeling of the background to stabilize R-factor values.

Low-temperature X-ray diffraction measurements of $Pb_{2/3}FeZr(PO_4)_{7/3}(SO_4)_{2/3}$ sample were taken on the same diffractometer in the temperature range 153–473 K at 40–50 K intervals using Anton Paar TTK 450 thermal accessory. Cooling effect was obtained with controlled flow of liquid nitrogen. Temperature was monitored with resistance thermometer Pt100 RTD. Range of diffraction angels was constant at each selected temperature ($2\theta = 10°-50°$). Si was used as external standard.

DTA–TG combined analysis of precursor and the prepared sample has been performed in argon atmosphere with DSC calorimeter Labsys TG–DTA/DSC in the temperature range 298–1473 K with heating and cooling speed 10 K min^{-1}. Analysis was performed in alundum crucible. Sample mass was 0.0815 g.

Functional composition of the sample was confirmed by IR-spectroscopy on a Shimadzu FTIR 8400S spectrometer within the range of 400–1400 cm^{-1}.

Results and discussion

Description of synthesis approach

Problem of synthesis of phosphate–sulfates emerges, due to considerable difference in thermal properties of phosphates and sulfates. Usually temperatures of phosphate synthesis are quite high (above 1023 K). Meanwhile, all sulfates (except A_2SO_4, BSO_4, A—alkaline, B—alkaline earth elements) are thermally unstable (usually stable below 873 K). So, if any unstable intermediate sulfate forms, there is a great chance that synthesis will not be done successfully, due to sulfur elimination from reaction zone and further violation of stoichiometry. Mixed phosphate–sulfate $Pb_{2/3}FeZr(PO_4)_{7/3}(SO_4)_{2/3}$ with expected NZP structure have been predicted according to the crystallographic data. Substitution

$$Pb^{2+} + 2P^{5+} \rightarrow 2S^{6+} \left(\text{or } (1/3)Pb^{2+} + (2/3)P^{5+} \rightarrow (2/3)S^{6+}\right)$$

in the basic $PbFeZr(PO_4)_3$ leads to $Pb_{2/3}FeZr(PO_4)_{7/3}(SO_4)_{2/3}$ formation. In case of its synthesis, possible unstable sulfates are $Fe_2(SO_4)_3$ (decay temperature 753 K), $Zr(SO_4)_2$ (decay temperature 398 K). In order to prevent precursor from sulfur elimination, we made use of Pb cation as a binding component ($PbSO_4$, decay temperature 1443 K). Opted stoichiometry of the sample prevents primal mixture from sulfur losses, binding its entire amount in $PbSO_4$ (melting point above 1273 K). The maximal temperature of sample synthesis (1023 K) was chosen according to the DTA–TG data.

DTA–TG analysis in keeping with X-ray diffractometry

DTA–TG and X-ray analysis of intermediate mixture with $Pb_{2/3}FeZrP_{7/3}S_{2/3}O_{12}$ stoichiometry showed that endothermic effects were connected with decay of primal reagents, which form heterogeneous system (653–743 K), crystallization of required phosphate–sulfate (1023 K) and its gradual transformation into phosphate $PbFeZr(PO_4)_3$ at 1468 K (as a result of sulfur elimination) (Fig. 2).

According to the X-ray patterns, the main phase of sample was crystallized with small amount of admixture of Fe_2O_3 at 873 K. At 1053 K, the single phase $Pb_{2/3}FeZr(PO_4)_{7/3}(SO_4)_{2/3}$ with NZP structure formed.

SEM and electron microprobe analysis

The electron probe X-ray microanalysis results showed that sample grain sizes were about 5 μ (Fig. 3) and uniform in composition, which coincided with the expected one $Pb_{2/3}FeZrP_{7/3}S_{2/3}O_{12}$ within experimental uncertainty (Table 1).

Crystal structure

The Rietveld refinement of the step scan data was performed by the least square method using Rietan. Table 2 summarizes the measurement conditions, unit cell

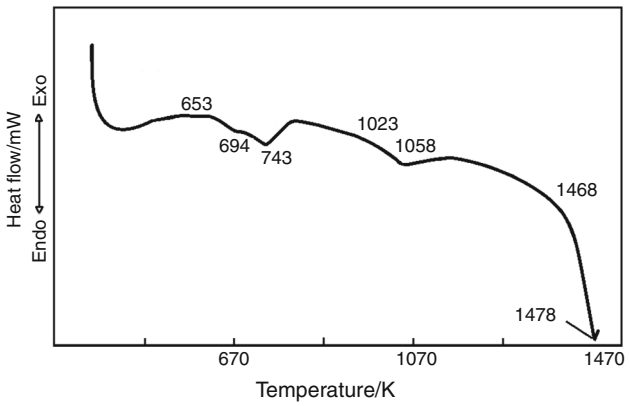

Fig. 2 DSC curve of $Pb_{2/3}FeZrP_{7/3}S_{2/3}O_{12}$ precursor

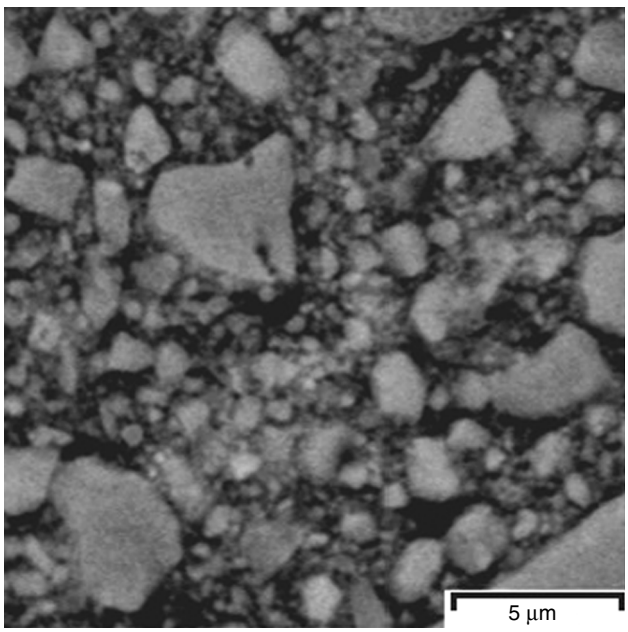

Fig. 3 SEM image of $Pb_{2/3}FeZr(PO_4)_{7/3}(SO_4)_{2/3}$ phosphate–sulfate

parameters and main data of the structure refinement. Figure 4 presents fragments of the experimental, calculated and difference X-ray diffraction patterns, as well as the line diagram of the diffraction pattern of the phosphate–sulfate. Assuming that $Pb_{2/3}FeZr(PO_4)_{7/3}(SO_4)_{2/3}$ belongs to the NZP family, Zr and Fe, P and S and O atoms are in the 12c, 18e and 36f Wyckoff positions, respectively, of the $R\bar{3}c$ space group. The Pb atoms were assumed to occupy the M1 sites. The refinement leads to a rather good agreement between the experimental and calculated diffraction pattern and yields acceptable reliability factors (R_p, R_{wp}) (Table 2). The main interatomic distances for the coordination polyhedral, forming the crystal structures of compound ($d_{Pb–O2} = 2.744(7)$, $d_{(Fe,Zr)–O1} = 1.775(5)$, $d_{(Fe,Zr)–O2} = 2.016(6)$, $d_{(P,S)–O1} = 1.691(8)$, $d_{(P,S)–O2} = 1.554(5)$ Å) are in a good agreement with the corresponding published data for phosphates and sulfates of a similar structure [26, 27]. The phosphate–sulfate consists of a framework formed by FeO_6-, ZrO_6-octahedra and SO_4-, PO_4-tetrahedra connected by vertices via Zr–O–P, Fe–O–P, Zr–O–S and Fe–O–S structural bridges (Fig. 5). The main "building" block of this framework is domain comprised of two octahedra and three tetrahedra arranged into columns. In $Pb_{2/3}FeZr(PO_4)_{7/3}(SO_4)_{2/3}$, the columns of such domains are oriented along the crystallographic *c*-axis.

Table 1 Chemical composition of phosphate–sulfate $Pb_{2/3}FeZrP_{7/3}S_{2/3}O_{12}$

Element	C_{at}^{theor}/%	$C_{at}^{virtually}$/%
Pb	3.77	3.59
Fe	5.66	4.45
Zr	5.66	5.16
P	13.21	14.25
S	3.77	3.50
O	67.92	69.05

FTIR-spectra

IR-spectrum of $Pb_{2/3}FeZr(PO_4)_{7/3}(SO_4)_{2/3}$, crystallizing in NZP structural type is shown in Fig. 6. In the space group $R\bar{3}c$(factor group D_{3d}), ions PO_4^{3-} and SO_4^{2-} are on 2-axis (positional symmetry C_2). Selection rules enable five asymmetric stretching ν_3, one symmetric stretching ν_1, five

Table 2 Summary of crystallographic data for $Pb_{2/3}FeZr(PO_4)_{7/3}(SO_4)_{2/3}$ compound

Formula	$Pb_{2/3}FeZr(PO_4)_{7/3}(SO_4)_{2/3}$
Structural analogue	$PbFeZr(PO_4)_3$
Crystal system	Trigonal
Space group	$R\bar{3}c$ (No. 167)
Z	6
Unit cell parameters:	
a/Å	8.6339 (4)
c/Å	23.2991 (9)
V/Å^3	1504.1 (1)
d_{calc}/g cm^{-3}	4.159 (1)
2θ angular range/°	10–110
Total number of reflections	214
Number of refined parameters	28
R_{wp}/%	3.24
R_p/%	2.20
S	2.9103

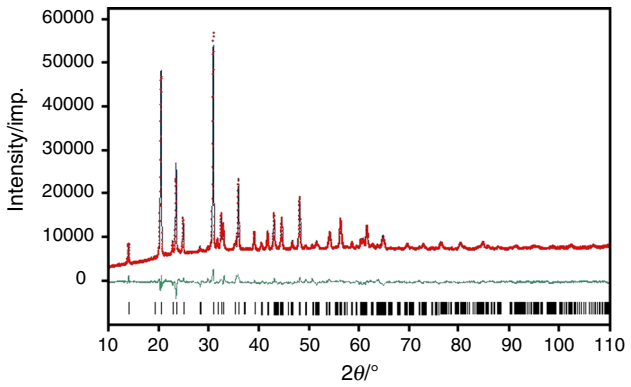

Fig. 4 Fragments of the (*blue*) experimental, (*red dots*) calculated, and (*green*) difference X-ray diffraction patterns, and (*black*) line diagram of $Pb_{2/3}FeZr(PO_4)_{7/3}(SO_4)_{2/3}$ phosphate–sulfate diffraction pattern

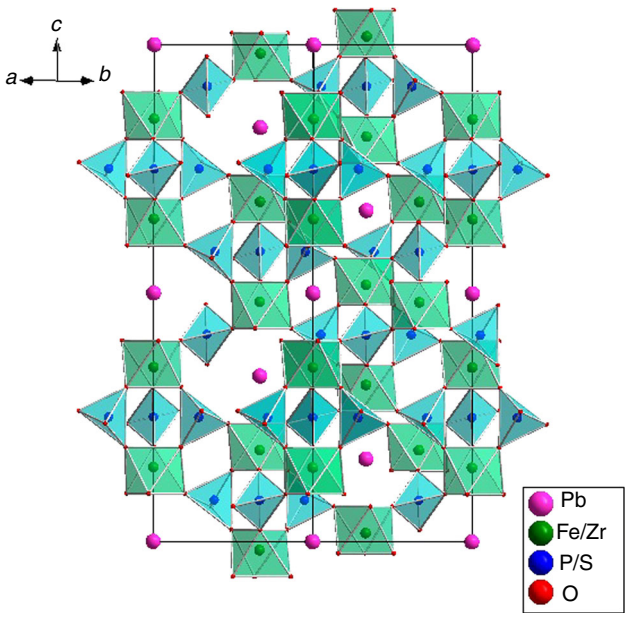

Fig. 5 Crystal structure of $Pb_{2/3}FeZr(PO_4)_{7/3}(SO_4)_{2/3}$ (*spring green* $(Fe/Zr)O_6$-octahedra, *cyan* $(P/S)O_4$-tetrahedra) (for interpretation of the references to color in this figure legend, the reader should refer to the web version of this article)

asymmetric bending v_4, two symmetric bending bands v_2 for each tetrahedral ion. Absorption bands in range 1220–1000 cm^{-1} are related to asymmetric stretching vibrations ν_3 of $(P,S)O_4$ ion. Emergence of high-frequent band 1204 cm^{-1} is explained by contribution of the electron density of Fe^{3+} and Zr^{4+} ions, which have small size and big charge. Band $\sim$ 957 cm^{-1} was related to symmetric stretching ν_1 vibration. Bands in range 640–550 cm^{-1} were related to bending ν_4 vibration, whereas 424 cm^{-1} to bending vibration ν_2 of $(P,S)O_4$ ion. The values of vibration wavenumbers of S–O and P–O

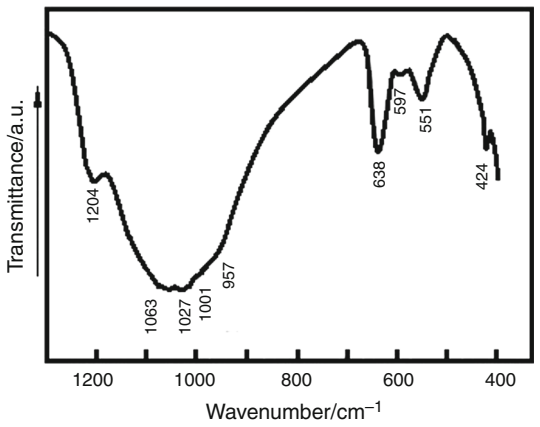

Fig. 6 FTIR transmittance spectra of $Pb_{2/3}FeZr(PO_4)_{7/3}(SO_4)_{2/3}$

bonds are identical, due to negligible difference between oxidation degrees of sulfur and phosphorus and resemblance between values of interatomic distances (for S–O and P–O bonds) and mass numbers of P and S.

Thermal expansion

Thermal expansion of $Pb_{2/3}FeZr(PO_4)_{7/3}(SO_4)_{2/3}$ was studied. The dependences between lattice parameters *a, c* and temperature are depicted in the Fig. 7. In accordance with them, it can be inferred that both of lattice parameters grow with increasing of temperature. It is caused by correlated rotation of $(Fe,Zr)O_6$-octahedra and $(P,S)O_4$-tetrahedra around *c*-axis, usual for NZP compounds. It is known that thermal expansion directly affects the average kinetic energy of the vibrating particles in a body and the average distances between the crystal lattice points and is related to the asymmetry (anharmonicity) of the thermal vibrations of atoms; as a result, under variable temperature conditions, the interatomic distances change. Research of thermal

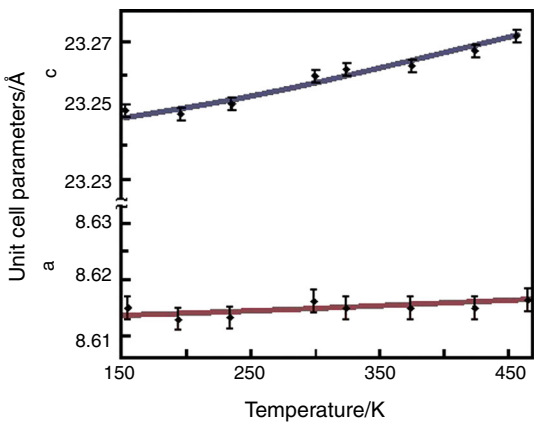

Fig. 7 Temperature dependence of $Pb_{2/3}FeZr(PO_4)_{7/3}(SO_4)_{2/3}$ unit cell parameters (crimson: *a*, blue: *c*)

deformations of crystal phosphate–sulfate structure revealed that direction of the biggest thermal expansion corresponds to c-axis ($\alpha_c > \alpha_a$). When $Pb_{2/3}FeZr(PO_4)_{7/3}(SO_4)_{2/3}$ compound is heated, more feeble Pb–O bonds elongate more than the strong (Zr,Fe)–O and (P,S)–O ones. Under heating, the size of the trigonal antiprism around the Pb site (M1 sites, see Fig. 5) increases and elongates the column of polyhedra along the c-axis ($\alpha_c > 0$); as a result, the $(Zr,Fe)O_6$-octahedra and $(P,S)O_4$-tetrahedra which share corners rotate, causing angular distortions in the polyhedra. The tetrahedral O–(P,S)–O angle increases along the c-axis, the distance between the columns of the framework structure shrinks, and the structure compresses along the a-axis. Nevertheless, under heating thermal deformations of quite strong O–O bonds along a-axis of various polyhedra, forming framework cause elongation; therefore, we can detect minimal thermal expansion of structure along a-direction. The values of the linear coefficients of thermal expansion are the following: $\alpha_a = 0.97 \cdot 10^{-6}$, $\alpha_c = 3.24 \cdot 10^{-6}$, $\alpha_{av} = 1.72 \cdot 10^{-6}$ K^{-1}. This phosphate–sulfate relates to the low expansion compositions group. Both of the coefficients α_a and α_c are positive; thus, it leads to relatively low anisotropy: $\alpha_c - \alpha_a = 2.27 \cdot 10^{-6}$ K^{-1}. For example, the axial coefficients in phosphate series $AE_2(PO_4)_3$ (A = Na, K, Rb, Cs; E = Zr, Hf), in the temperature range from 123 to 1073 K, are within the limits: $\alpha_a = (-5.5 \text{ to } 0.3) \cdot 10^{-6}$ K^{-1}, $\alpha_c = (23.5 \text{ to } -0.9) \cdot 10^{-6}$ K^{-1} moving along the raw from the composition with Na (ionic radius $r_{Na^+} = 1.02$ Å) to the composition with Cs (ionic radius $r_{Cs^+} = 1.67$ Å) [3, 28]. As we expected before, directional combination of varied tetrahedral anions in NZP compounds (PO_4^{3-} and SO_4^{2-}) caused reducing size of framework and its cavities. That afforded us to obtain low-expanding phosphate–sulfate with extra-framework lead cation, which smaller than conventionally used ones (with bigger size) in monoanion phosphates.

Conclusions

We suggested new synthesis method of phosphate–sulfates and proved it by $Pb_{2/3}FeZr(PO_4)_{7/3}(SO_4)_{2/3}$ formation. Also we have determined the thermal expansion parameters of the phosphate–sulfate with NZP structure. So, compound related to materials with ultra-low thermal expansion.

In accordance with represented method, it may be easily applied to other compounds, which synthesis can be performed via formation of intermediate sulfate with high melting temperature. We are on a verge of the synthesis of the following row: $Pb_{2-0.5x}MgFe(PO_4)_{3-x}(SO_4)_x$ ($0 < x < 4/3$). It is appealing because of the maintenance of lead excess in comparison with sulfur. It offers an opportunity to completely bind sulfur in precursor and finally synthesize phosphate–sulfates.

Acknowledgements The present work was performed at the Lobachevsky State University of Nizhni Novgorod with the financial support of the Russian Foundation for Basic Research (Project No. 15-03-00716 a).

References

1. Pet'kov VI, Asabina EA, Sukhanov MV, Schelokov IA, Shipilov AS, Alekseev AA. Design and characterization of phosphate-containing ceramics with Kosnarite- and Langbeinite-type structures for industrial applications. Chem Eng Trans. 2015;43:1825–30.
2. Anantharamulu N, Koteswara Rao K, Rambabu G, Vijaya Kumar B, Radha V, Vithal M. A wide-ranging review on Nasicon type materials. J Mater Sci. 2011;46:2821–37.
3. Pet'kov VI. Complex phosphates formed by metal cations in oxidation states I and IV. Russ Chem Rev. 2012;81:606–37.
4. Arbi K, Bucheli W, Jimenez R, Sanz J. High lithium ion conducting solid electrolytes based on NASICON $Li_{1+x}Al_xM_{2-x}(PO_4)_3$ materials (M = Ti, Ge and $0 \le x \le 0.5$). J Eur Ceram Soc. 2015;35:1477–84.
5. Pet'kov VI, Asabina EA, Shchelokov IA. Thermal expansion of NASICON materials. Inorg Mater. 2013;49:502–6.
6. Bohre A, Awasthi K, Shrivastava OP. Immobilization of lanthanum, cerium, and selenium into ceramic matrix of sodium zirconium phosphate. Radiochemistry. 2014;56:385–91.
7. Kim J, Jo SH, Bhavaraju S, Eccleston A, Kang SO. Low temperature performance of sodium–nickel chloride batteries with NASICON solid electrolyte. J Electroanal Chem. 2015;759:201–6.
8. Pet'kov V, Asabina E, Loshkarev V, Sukhanov M. Systematic investigation of the strontium zirconium phosphate ceramic form for nuclear waste immobilization. J Nucl Mater. 2016;471:122–8.
9. Ilin AB, Orekhova NV, Ermilova MM, Yaroslavtsev AB. Catalytic activity of $LiZr_2(PO_4)_3$ nasicon-type phosphates in ethanol conversion process in conventional and membrane reactors. Catal Today. 2016;268:29–36.
10. Ivanov-Shitz AK, Murin IV. Ionika tverdogo tela (Solid-State Ionics). St. Petersburg: Gos. Univ; 2001.
11. Pérez-Estébanez M, Isasi-Marín J, Többens DM, Rivera-Calzada A, León C. A systematic study of Nasicon-type $Li_{1+x}M_xTi_{2-x}(PO_4)_3$ (M: Cr, Al, Fe) by neutron diffraction and impedance spectroscopy. Solid State Ion. 2014;266:1–8.
12. Ortiz GF, López MC, Lavela P, Vidal-Abarca C, Tirado JL. Improved lithium-ion transport in NASICON-type lithium titanium phosphate by calcium and iron doping. Solid State Ion. 2014;262:573–7.
13. Liu XS, Li F, Song WB, Yuan BH, Cheng YG, Liang EJ, et al. Control of reaction processes for rapid synthesis of low-thermal-expansion $Ca_{1-x}Sr_xZr_4P_6O_{24}$ ceramics. Ceram Int. 2014;40:6013–20.
14. Pet'kov VI, Shipilov AS, Sukhanov MV. Thermal Expansion of $MZr_2(AsO_4)_3$ and $MZr_2(TO_4)_x(PO_4)_{3-x}$ (M = Li, Na, K, Rb, Cs; T = As, V). Inorg Mater. 2015;51:1179–85.
15. Pet'kov VI, Orlova AI. Crystal chemical approach to predicting the thermal expansion of compounds in the NZP family. Inorg Mater. 2003;39:1013–23.
16. Pet'kov VI, Orlova AI, Kasantsev GN, Samoilov SG, Spiridonova ML. Thermal expansion in the Zr and 1-, 2-valent complex phosphates of $NaZr_2(PO_4)_3$ (NZP) structure. J Therm Anal Calorim. 2001;66:623–32.

17. Oikonomou P, Dedeloudis C, Stournaras CJ, Ftikos C. [NZP]: a new family of ceramics with low thermal expansion and tunable properties. J Eur Ceram Soc. 2007;27:1253–8.
18. Pet'kov VI, Asabina EA. Thermophysical properties of NZP ceramics (a review). Glass Ceram. 2004;61:233–9.
19. Lenain GE, McKinstry HA, Alamo J, Agraval DK. Structural model for thermal expansion in $MZr_2P_3O_{12}$ (M = Li, Na, K, Rb, Cs). J Mater Sci. 1987;22:17–22.
20. Pet'kov VI, Asabina EA, Markin AV, Smirnova NN. Synthesis, characterization and thermodynamic data of compounds with NZP structure. J Therm Anal Calorim. 2007;91:155–61.
21. Malecki S. Reduction of lead and zinc sulfates by hydrogen. J Therm Anal Calorim. 2015;121:861–6.
22. Dey A, Das Gupta A, Basu D, Ambashta RD, Wattal PK, Kumar S, Sen D, Mazumber S. A comparative study of conventionally sintered, microwave sintered and hot isostatic press sintered NZP and CZP structures interacted with fluoride. Ceram Int. 2013;39:9351–9.
23. Kim Y-I, Izumi F. Structure refinements with a new version of the Rietveld-refinement program RIETAN. J Ceram Soc Jpn. 1994;102:401–4.
24. Rietveld HM. Line profiles of neutron powder-diffraction peaks for structure refinement. Acta Crystallogr. 1967;22:151–2.
25. Izumi F. The Rietveld method. Young RA, editor. Oxford: Oxford Univ. Press; 1993.
26. Eremin NN, Sukhanov MV, Pet'kov VI, Urusov VS. Interatomic potentials for structural modeling of double alkali-metal zirconium orthophosphates. Dokl Chem. 2004;396:107–10.
27. Piffard Y, Verbaere A, Kinoshita M. β-$Zr_2(PO_4)_2SO_4$: a zirconium phosphato-sulfate with a $Sc_2(WO_4)_3$ structure. A comparison between garnet, nasicon, and $Sc_2(WO_4)_3$ structure types. J Solid State Chem. 1987;71:121–30.
28. Miyazaki H, Ushiroda I, Itomura D, Hirashita T, Adachi N, Ota T. Thermal expansion of $NaZr_2(PO_4)_3$ family ceramics in a low-temperature range. Jpn J Appl Phys. 2008;47:7262–5.